agronomy

MDPI

Article

Trend Prediction of Vegetation and Drought by Informer Model Based on STL-EMD Decomposition of Ha Cai Tou Dang Water Source Area in the Maowusu Sandland

Hexiang Zheng [1], Hongfei Hou [1,2], Ruiping Li [2,*] and Changfu Tong [1,*]

[1] Institute of Pastoral Water Resources Science, Ministry of Water Resources, Huhhot 010020, China; mkszhx@163.com (H.Z.)
[2] College of Water Conservancy and Civil Engineering, Inner Mongolia Agricultural University, Huhhot 010018, China
* Correspondence: nmglrp@imau.edu.cn (R.L.); tongcf@iwhr.com (C.T.)

Abstract: To accurately forecast the future development trend of vegetation in dry areas, it is crucial to continuously monitor phenology, vegetation health indices, and vegetation drought indices over an extended period. This is because drought caused by high temperatures significantly affects vegetation. This study thoroughly investigated the spatial and temporal variations in phenological characteristics and vegetation health indices in the abdominal part of Maowusu Sandland in China over the past 20 years. Additionally, it established a linear correlation between vegetation health and temperature indices in the arid zone. To address the issue of predicting long-term trends in vegetation drought changes, we have developed a method that combines the Informer deep learning model with seasonal and Seasonal Trend decomposition using Loess (STL) and empirical mode decomposition (EMD). Additionally, we have utilized the linearly correlated indices of vegetation health and meteorological data spanning 20 years to predict the Normalized Difference Vegetation Index (NDVI) and Temperature Vegetation Dryness Index (TVDI). The study's findings indicate that over the 20-year observation period, there was an upward trend in NDVI, accompanied by a decrease in both the frequency and severity of droughts. Additionally, the STL-EMD-Informer model successfully predicted the mean absolute percentage error (MAPE = 1.16%) of the future trend in vegetation drought changes for the next decade. This suggests that the overall health of vegetation is expected to continue improving during that time. This work examined the plant growth circumstances in dry locations from several angles and developed a complete analytical method for predicting long-term droughts. The findings provide a strong scientific basis for ecological conservation and vegetation management in arid regions.

Keywords: drought; TVDI; phenology; long-series trend; the STL-EMD-Informer model

Citation: Zheng, H.; Hou, H.; Li, R.; Tong, C. Trend Prediction of Vegetation and Drought by Informer Model Based on STL-EMD Decomposition of Ha Cai Tou Dang Water Source Area in the Maowusu Sandland. *Agronomy* **2024**, *14*, 708. https://doi.org/10.3390/agronomy14040708

Academic Editors: Anna Tedeschi and Rodolfo Gentili

Received: 18 February 2024
Revised: 23 March 2024
Accepted: 27 March 2024
Published: 28 March 2024

1. Introduction

The fundamental element of terrestrial ecosystems is vegetation, but as a result of increased global warming and human activity, climatic extremes like droughts are occurring more frequently. This has resulted in a decline in the health of the ecosystem and a reduction in the amount of vegetation cover, which has far-reaching global implications [1]. To combat drought and lessen vegetation loss, remote sensing technology has proven essential in monitoring changes in the vegetation, particularly over extended periods and at large scales [2].

The Maowusu Sandland in Inner Mongolia is an area characterized by low plant cover and delicate ecosystems, where climate variables have caused extensive vegetation degradation [3]. The primary factors contributing to the drought are arid climate and little rainfall. The majority of locations see an annual precipitation of less than 440 mm, with some areas receiving even less than 200 mm. Due to the concentration of precipitation in

July, August, and September, together with the arid environment and rapid evaporation, the humidity fluctuates significantly throughout the year, leaving it susceptible to droughts and windstorms [4]. The Normalized Difference Vegetation Index (NDVI), which can be used to analyze both the temporal and geographical variations in vegetation as well as the vegetation's sensitivity to climate change, is one of the key instruments associated with this phenomenon [5]. Since a decline in NDVI values is a common sign of plant degradation, obtaining and interpreting NDVI data is crucial to comprehending the regional vegetation dynamics of the Maowusu Sandland [6].

The Temperature Vegetation Dryness Index (TVDI) is a useful tool for visually assessing the degree of dryness and determining the status of vegetation [7]. TVDI is crucial for tracking the dynamics of widespread, multitemporal droughts and offers a solid scientific foundation for predicting future droughts, both of which may enhance the amount and quality of vegetation [8]. While many researchers have used Landsat and MODIS data to predict TVDI for interannual interpolation of Landsat TVDI data and assessment of vegetation condition in recent years, there is still a lack of research on long-term series prediction and the dominant drivers of vegetation change in arid and semi-arid zones. Most of the studies that have been conducted so far have mostly focused on how vegetation zones are responding to climate change [9]. Lin et al. state that in remote sensing approaches based on drought indicators, the Temperature Condition Index (TCI) is based on surface temperature, while the Vegetation Condition Index (VCI) is supported by NDVI [10]. According to Oliveira et al., these two indicators make it possible to monitor the length, severity, and effects of drought on vegetation changes with more accuracy [11]. Specifically, large-scale droughts and their impacts on vegetation may be monitored using the Vegetation Health Index (VHI) and the VCI, particularly in research that examines the relationship between crop output and agricultural drought [12]. Concurrently, VCI and TCI work better together than they do alone, which encourages the growth of VHI. Furthermore, a more intuitive response to vegetation growth is offered by the Vegetation Water Supply Index (VSWI), which is based on land surface temperature (LST) and the NDVI [12].

In the field of global change research, quantifying the factors causing vegetation change and forecasting future patterns are popular topics [13]. Through a thorough analysis of drought conditions and vegetation health, we may obtain a deeper and more exact understanding of vegetation change. The complexity of model optimization and the limitations of computational speed remain the main challenges for machine learning models, such as random forest, support vector machine (SVM), and support vector regression (SVR), which are currently widely used to predict trends despite their effectiveness in predicting vegetation metrics [14]. For instance, Lin et al. used LST and the NDVI to characterize large-scale drought conditions [15]. The correlation with soil moisture can be better derived through the TVDI, and this is widely used in remote sensing drought, which is suitable for long time-series analysis [15]; Gidey et al. effectively improved the NDVI in-version accuracy through the use of the SVR algorithm, although the model has several drawbacks, including a slow convergence speed and a highly complex optimization process [16]. Chen et al. introduced an SVM model to simulate the quantification of the effect of LST on vegetation cover, but there were machine learning shortcomings. Due to its strong learning and fitting capabilities, deep learning has emerged as a viable alternative to conventional statistical and machine learning techniques for handling large-scale time series data, particularly for short-term TVDI prediction [17].

Although the prediction accuracy has improved, deep learning techniques like deep neural networks (DNN), deep belief networks (DBN), convolutional neural networks (CNN), and recurrent neural networks (RNN) still have limitations when it comes to complex nonlinear time-series data prediction [18]. To thoroughly examine how the NDVI responds to climatic conditions, Gao et al. used CNN to develop an NDVI prediction model, which significantly increased the NDVI forecast's accuracy [18]. However, when working

with data that are very volatile and non-stationary, CNN's prediction accuracy drops [19]. Although RNN effectively extracts the NDVI data for fitting and adds a cyclic structure that can better handle time-series data, RNN has limitations, including the inability to capture long-term relationships and disappearing gradients [20]. However, according to Li et al., RNN has issues such as gradient vanishing and is unable to capture long-term relationships [21]. In short-term TVDI prediction tasks, the long short-term memory (LSTM) network, a unique sort of RNN, outperforms RNN; nevertheless, LSTM has issues with many parameters and sluggish model convergence [22]. The Transformer model has been proposed and used in the field of time series prediction in recent years. However, despite producing better predictions, the Transformer model is time- and resource-consuming due to its high memory occupancy and complexity [23]. The temporal series prediction has recently seen new opportunities thanks to the Transformer and Informer models; in particular, the Informer has made great strides in resolving the Transformer's memory occupancy and temporal complexity [24]. This paper addresses three issues with the previous Transformer: (1) the memory bottleneck of the long-time input stacking layer; (2) the complexity and memory usage of the self-attention mechanism; and (3) the speed degradation of predicting long output time series. The Informer model proposal addresses the shortcomings of the Transformer. In addition to demonstrating outstanding potential in long-time series input and output dependencies, the improved Informer model can effectively improve the LSTF problem's prediction ability. It also introduces the probabilistic sparse self-attention mechanism, which can effectively reduce the complexity of its space.

We suggest combining the secondary decomposition approach with a deep learning model (Informer) to increase the prediction accuracy even further. By breaking down the original data into parts and using secondary analysis to retrieve relevant information and inherent rules, this strategy increases prediction accuracy [25]. Wu et al. employed VMD to decompose short-term electricity load data and reconstructed the prediction results to achieve better prediction results [26]. Zhang et al. performed VMD secondary decomposition on the components obtained from EMD based on the samples, which increased the accuracy of the prediction results [27]. While the secondary decomposition method can further refine the data and optimize the prediction model, most current studies are still limited to the primary decomposition, which results in residual components that still contain a significant amount of non-stationarity despite the decomposition technique's effectiveness in reducing non-stationarity and complexity of the data [28]. However, the decomposed characteristics of the current quadratic decomposition models are not thoroughly analyzed, which results in inadequate information extraction and lowers prediction accuracy [29]. Our goal is to improve these decomposition techniques so that vegetation change may be predicted with greater accuracy.

This work uses the Google Earth Engine (GEE) cloud platform with 20 years of multiple change analysis and attribution algorithms to develop a complete vegetation pre-restoration analysis system in the present context of global warming and growing drought. To give strong scientific backing for the building of an ecological environment restoration in the Ha Cai Tou Dang water source region, the system seeks to thoroughly uncover and evaluate the connection between vegetation and climate. The details of our methodology structure diagram are shown in Figure 1. The main objectives of this study include: (1) in the context of an ecological restoration project with global warming and gradual intensification of aridification, to study in depth the interaction relationship between vegetation dynamics and spatial and temporal changes in climate under the condition of natural restoration by taking the trend change of NDVI and the cycle of phenology growth as a starting point; (2) to assess the unique contribution of natural restoration to vegetation change by taking the Ha Cai Tou Dang water source area water source area as a research object and to analyze the spatiotemporal variation of TVDI and the performance of VSWI, VCI, TVDI, and VHI in different growing seasons so as to optimize the application of these metrics in the study of vegetation drought; and (3) to propose, by combining 20 years of meteo-

rological, NDVI, and TVDI data, a new model based on the Seasonal Trend Transitional Decomposition (STL), the Empirical Modal Decomposition (EMD), and the Informer model in order to provide a strong scientific basis for ecological environmental protection and sustainable development.

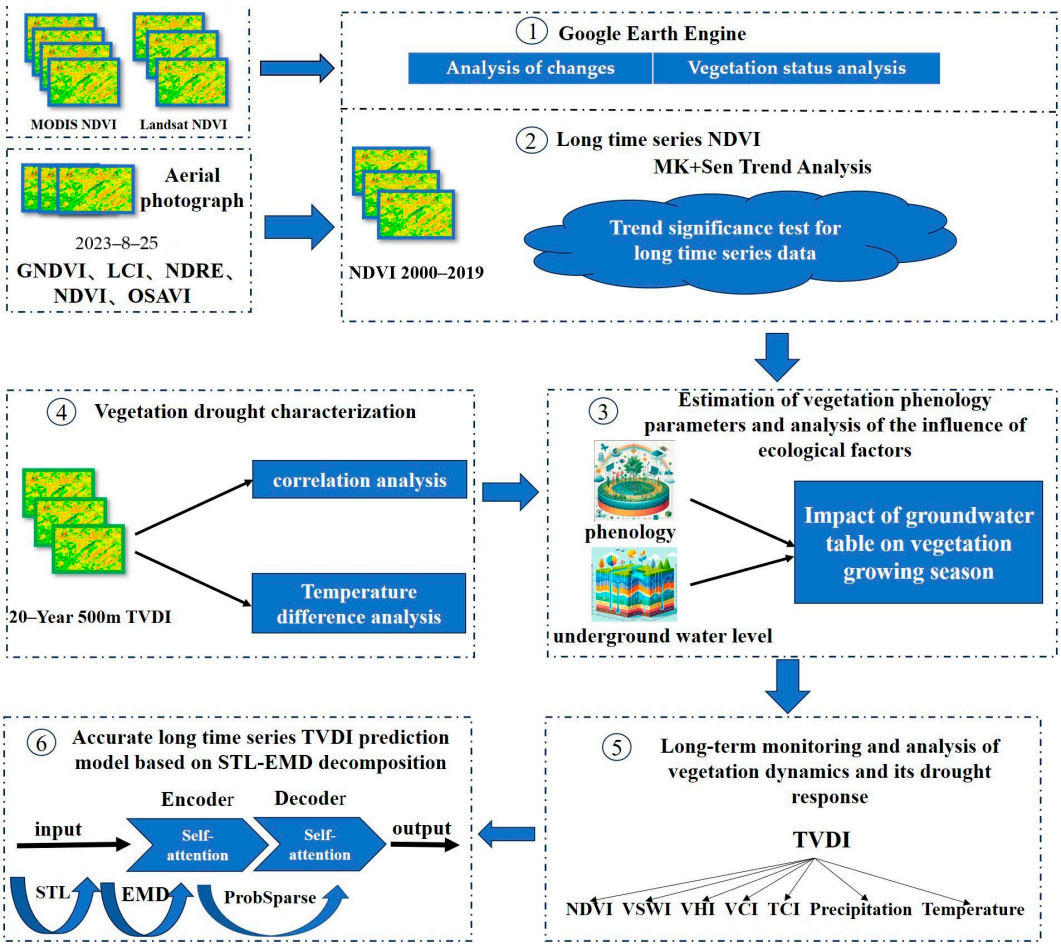

Figure 1. Methodology flowchart.

2. Materials and Methods

2.1. Study Area

The Ha Cai Tou Dang water source area is located in the belly of the Maowusu sandland area, which experiences semiarid and desert conditions, in northwest China. The area spans around 2986 square kilometers, with high topography in the eastern region and lower topography in the western region (Figure 2 illustrates the geographic location and elevation of the study area). The location is situated in Wushen Banner, Ordos City, Inner Mongolia Autonomous Region, within the coordinates of (108°83′–109°68′ E, 38°32′–39°10′ N). The water source of Ha Cai Tou Dang has a moderate continental monsoon climate, characterized by average annual temperatures ranging from 6.0 to 8.5 °C, precipitation levels of 220–400 mm, evaporation rates of 2100–2600 mm, and an average annual wind speed of 4.5 m/s. The climate of the Ha Cai Tou Dang water source area is characterized by significant evaporation, a fluctuating distribution of precipitation, intense solar radiation, windy and sandy conditions, and aridity [29].

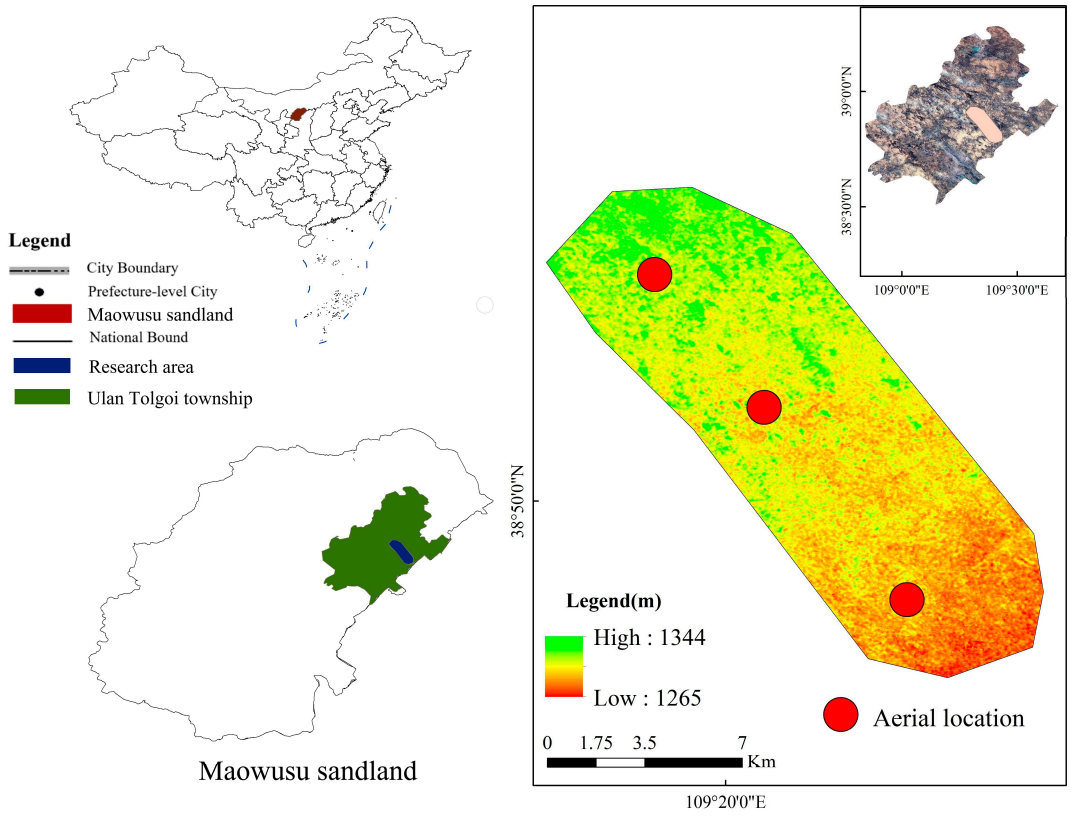

Figure 2. Ha Cai Tou Dang water source area geographic location.

2.2. Data and Processing

2.2.1. Field Investigation

The experiment acquired data from the water source area of Ha Cai Tou Dang in Wulan Tolgoi Town, Wushen Banner, Erdos City, Inner Mongolia. The coordinates of the location are 109°16′–109°26′ E, 38°46′–39°55′ N. The NDVI data were collected using a DJI Wizard 4 multispectral drone equipped with a 20 mm lens focal length, a −90°~30° lens imaging angle, 20 um pixel size, and a picture resolution of 400 × 3000 pixels. The unmanned aerial vehicle (UAV) maintained an altitude of 90–100 m while following an S-shaped path. Figure 2 illustrates the positions of the aerial photographs. The DJI 3D modeling application was used to combine hyperspectral photos. The system categorized several hyperspectral samples by similarity, elevation data, and aerial film coordinates. Subsequently, it generated superior splices and synthesized file naming and delivery.

2.2.2. Remote Sensing Data Source

The GEE cloud platform was utilized to eliminate the limitations of time and space in the geomorphological study. This involved generating long time series and conducting multi-year mean analysis using the Landsat series. The resulting dataset consisted of NDVI values with a spatial resolution of 250 m, derived from remote sensing data collected over an extended period in the study area.

The data from the Moderate Resolution Imaging Spectroradiometer (MODIS), as well as the NDVI, TVDI, VSWI, VHI, VCI, and TCI, were obtained from the GEE platform (https://earthengine.google.com/) (accessed on 23 December 2023). Quantitative analysis was used to assess changes in plant cover and the drought index within the Hacai Tou water source area. The datasets employed had a monthly temporal resolution and a spatial resolution of 500 m. These datasets included MOD13Q1, MOD11A2 NDVI, LST, TVDI, VSWI, VHI, TCI, and VCI. The picture with monthly temporal resolution spanning the years 2000–2020 was created by using the highest pixel value. The photos were created

using the average synthesis technique, which included employing impact data obtained from January to December. In addition, each year throughout the study period, the Landsat images were analyzed at the pixel level to calculate the annual 95th quantile synthesis. This process helped to reduce the uncertainty caused by the limited number of images available each year [30].

2.2.3. Elevation and Land Use Data Sources

The selection of digital elevation model (DEM) data was made from the geospatial data cloud (https://www.gscloud.cn/) (accessed on 15 November 2023) using ASTER DEM 30M resolution digital elevation data. The DEM data were analyzed and the elevation was determined using ArcGIS 10.8.

The Globeland30 dataset, which is a global land cover dataset generated in China, included three years of land use data: 2000, 2010, and 2020. The data were collected at a resolution of 30 m. The many types of land included barren terrain, grassland, agriculture, shrubland, wetland, aquatic bodies, woodland, and man-made surfaces.

2.2.4. Hydroclimatological Information

The primary source of meteorological data for this inquiry was the fifth-generation ECMWF Atmospheric Reanalysis (ERA5) dataset obtained from the GEE cloud platform. The ERA5 dataset contains daily mean temperature and daily precipitation data from 2000 to 2019, with a precision of 27,830 m. The data were calculated using the total_precipitation band and the mean_2m_air_temperature band using hourly temperature data at a height of 2 m above the ground.

2.3. Research Methodology

2.3.1. MK + Sen Trend Analysis

Nonparametric approaches were used to analyze the temperature–rainfall time series for significant patterns. The Mann–Kendall and Sen slope estimators, known for their computational efficiency, were used to ascertain the trend and slope, respectively, due to the non-normal distribution of the temperature–rainfall data [31].

Sen's trend is a robust non-parametric statistical technique used to determine trends. It is not affected by measurement mistakes or outlier data. Conversely, the MK test does not need adherence to a particular distribution for the samples, is less influenced by extreme values, and is suitable for conducting important tests on patterns in extensive time series data [32]. The Theil–Sen and Mann–Kendall tests may be integrated to assess long-term vegetation time series.

The calculation formula is:

$$\beta = Median\left(\frac{x_j - x_i}{j - i}\right) \forall j > i \tag{1}$$

$$Var(S) = \frac{n(n-1)(2n+5)}{18} \tag{2}$$

$$Z = \begin{cases} \frac{S}{\sqrt{Var(S)}} \ (S > 0) \\ 0 \ (S = 0) \\ \frac{S+1}{\sqrt{Var(S)}} \ (S < 0) \end{cases} \tag{3}$$

where X_j and X_i are time series data. β is an indicator used to show the trend of a time series. β greater than 0 indicates an upward trend in the time series; β less than 0 indicates a downward trend in the time series. S is the statistic that calculates the trend in the data. Z is a statistic that tests for the presence of a monotonic trend in the data.

2.3.2. Lenvenberg–Marquardt Technique for Constructing Logistic Dual Models

To determine object quantities, we used automated object extraction methods and bi-logistic smoothing [33]. The dual logistic function shown below was used to predict the yearly growth pattern:

$$\int(t) = v1 + v2\left(\frac{1}{1+e^{-m_1(t-n_1)}} + \frac{1}{1+e^{-m_2(t-n_2)}}\right) \quad (4)$$

where $f(t)$ is the fitted EVI value at the day t; v is the background and amplitude of EVI over the entire year, respectively; the first sigmoid (Sig1: $\frac{1}{1+e^{-m_1(t-n_1)}}$) with pairparameters of m and n captures the green-up phase of vegetation growth; and the second sigmoid (Sig2: $\frac{1}{1+e^{-m_2(t-n_2)}}$) with pair-parameters of m and n captures the senescence phase of vegetation growth.

This logistic methodology automates the extraction of characteristics relevant to the six late afternoon seasonal changeover dates [33]. These include germination, season duration, maturity, season end, dormancy, and season termination. The model's spring growth and autumn senescence trajectories have the steepest slopes at the greatest and lowest values of the first-order derivative (SOS and EOS). Model inflection points, which are local maxima of the second-order derivative, coincide with the green stage, maturity, and dormancy [34]. A season's duration is the number of days between its start (SOS) and its end (EOS). The phenology of individual data sets may also be shown using seasonal variation and season-start and -finish rates.

2.3.3. Partial Mantel Test

We used the R programming language software, namely, version 4.2.3, to conduct a statistical analysis of the provided data. Before conducting the statistical analysis, we generated random seeds to ensure the replicability of the results. By using the "vegan" package, we performed Mantel tests to analyze the relationships between several factors, including rainfall climate, TVDI, NDVI, VSWI, VHI, TCI, and VCI. To determine the relationships between these indices, we divided the R-values and *p*-values of the Mantel test using the modified function [35]. Finally, to examine the link between these markers, we generated correlation heat maps. This approach enhances our comprehension and predictive ability about the impact of climate change on vegetation. It provides a valuable instrument for quantifying and visualizing the inter-relationships among various environmental variables.

2.3.4. Accurate Long-Time Series TVDI Prediction Model Based on STL-EMD Decomposition

The Transformer model is effective in addressing long-time series prediction issues because of its inherent multi-layer encoder structure. However, as the length of the series rises, the model's speed steadily decreases, which may impact its prediction effectiveness. The prediction results of TVDI periodic time series are particularly challenging due to the combined effects of time and variables. Additionally, the time series data associated with this prediction are generally intricate, noisy, and non-stationary. The study proposes the integration of the STL-EMD decomposition with the Transformer model, known as the STL-EMD-Informer (Figure 3), to overcome the limitations of the encoder–decoder design and effectively handle the identified concerns. This approach utilizes the LSTM model to enhance its performance. The time series is first decomposed by the model into trend, seasonality, and residual components. Subsequently, the residual component is decomposed into 10 intrinsic feature components (IMF_s) to further mitigate its variability. The encoder utilizes a probabilistic sparse self-attention mechanism to train and learn from sequences with greater probability in the input. This approach selects critical Q-values to reduce model complexity and improve prediction accuracy. Figure 3 shows in detail how our STL-EMD-Informer model works and the improvements made.

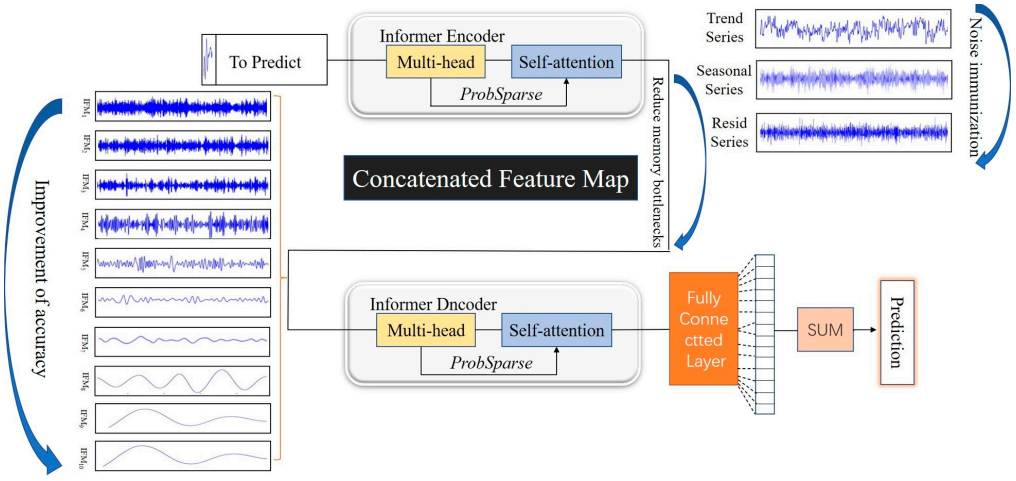

Figure 3. Schematic diagram of the STL-EMD-Informer model.

3. Results

3.1. Spatiotemporal Characteristics of Land Use Types

The land use categories in the Ha Cai Tou Dang water source area, from 2000 to 2020, ranked, in descending order of size, as follows: grassland, bare land, shrubland, farmland, and forest. From 2000 to 2010, the land use categories in the study region stayed mostly the same, except for a slight decline in grassland and a rather substantial rise in bare land. Between 2010 and 2020, there was a notable decline in the extent of grassland and a substantial rise in the extent of bare land. The regions classified as shrubland, farmland, and forest had few alterations.

Overall, the Ha Cai Tou Dang water source area has had sporadic periods of increased bare land and sporadic periods of decreased grassland (Figure 4 presents in detail the spatial distribution of land use types for the years 2000, 2010, and 2020). The agricultural land in the region is poorly distributed, mostly concentrated in the central section of the Ha Cai Tou Dang water source area. The restoration and conservation of the sandy land's ecosystem mostly depend on the use of grassland. Nevertheless, according to a 20-year field research study, there was no notable alteration in grassland and bare land in 2010. However, in 2020, there was a decline in the extent of pasture land in the study region, accompanied by an increase in the quantity of bare land. Indications point to a deterioration in the ecological condition of the region; please see Figure 5 for further reference. Figure 5 illustrates the changes in land use types over 20 years.

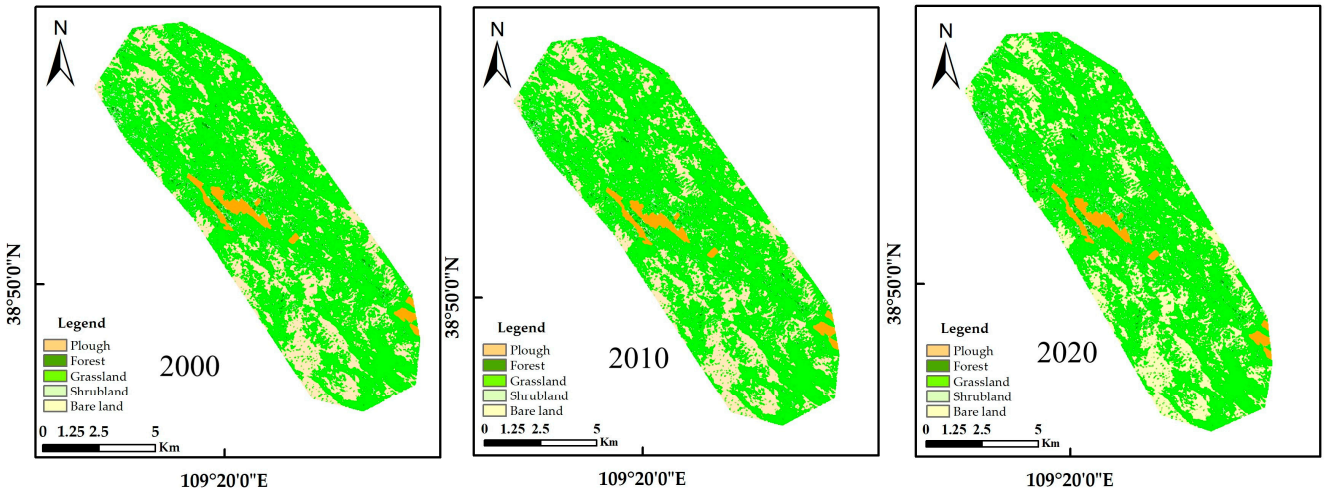

Figure 4. Land use type maps for the years 2000, 2010, and 2020.

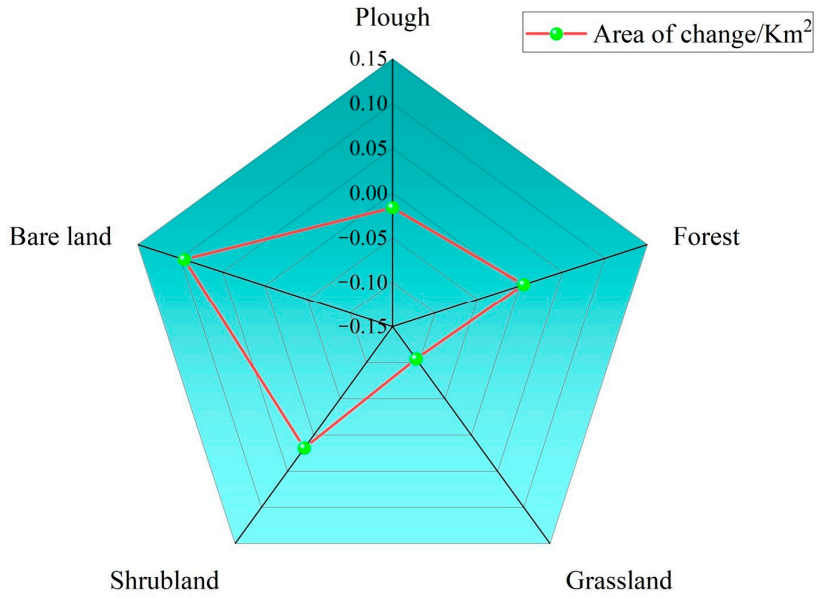

Figure 5. Map of changes in land use types: 2000, 2010, 2020.

The aforementioned data and observations indicate that changes in land use have a substantial influence on the ecological conditions of the Ha Cai Tou Dang water source area. To accomplish the ecological restoration and protection of the sandy land, modifying the land use plan in the area may help to improve its ecological environment. One way to accomplish this is by augmenting the extent of grassland while reducing the expanse of barren ground.

3.2. Trend Analysis of Vegetation Changes

The NDVI of the Ha Cai Tou Dang water source area was 0.18 between 2000 and 2019. The NDVI exhibited a consistent upward trend over the specified period, but with a diminished rate of growth. This was determined by the development of a linear regression equation, which yielded a slope of 0.003 a^{-1} (Figure 6 details the trends in NDVI over the last 20 years). The predominant factor contributing to the limited vegetation cover in the research area in 2000 was the significant presence of bare terrain in the Sandy Hinterland region. In the majority of locations, the vegetation cover was below 30%. Despite the continued presence of spatial disparities, the Ha Cai Tou Dang water source area has experienced notable enhancements in its ecological environment and augmentation in vegetation coverage in recent years. These improvements can be attributed to the implementation of ecological protection and construction initiatives by both Chinese and local governments. The ecological habitat of the Ha Cai Tou Dang water source area has seen enhancement and enhanced protection as a result of these measures.

The research region has low temperatures and cold weather throughout the winter months, which have a notable suppressive impact on plant development. Figure 7 clearly shows the average temperature and total annual rainfall for the period 2010–2019. Additionally, this severe climatic condition has a detrimental influence on agricultural yield. More precisely, this might result in a postponement of the beginning of plant development in the spring and an acceleration at the end of autumn, thereby reducing the duration of the growing season and impacting plant growth and reproduction. Furthermore, organisms that are sensitive to freezing temperatures may be unable to endure such conditions, potentially resulting in a reduction in biodiversity. Plants in the study region may undergo morphological changes, such as decreased body size, smaller leaves, and developed root systems, to adapt to the low temperature and cold environment. These modifications help limit heat loss and enable the plants to discover additional sources of water. The process of plant decomposition may be hindered, resulting in the buildup of apoplastic

material. This, in turn, has an impact on the soil's ability to cycle nutrients and retain water. Furthermore, the presence of low temperatures and cold conditions may impede the process of photosynthesis and respiration in plants, resulting in a decrease in their growth rate and the accumulation of biomass. The impacted plant state in the research region may limit the ecosystem service functions, including sand and wind retention, soil and water conservation, and provision of animal habitats. The research region is characterized by its ecological fragility and high sensitivity to low temperatures and cold. The development of plants in this area is significantly impacted by the climatic conditions. Nevertheless, the increase in temperature and moisture in the climate has significant practical implications for the expansion and density of plant life, the strategic management and usage of land, and the preservation of the ecological environment.

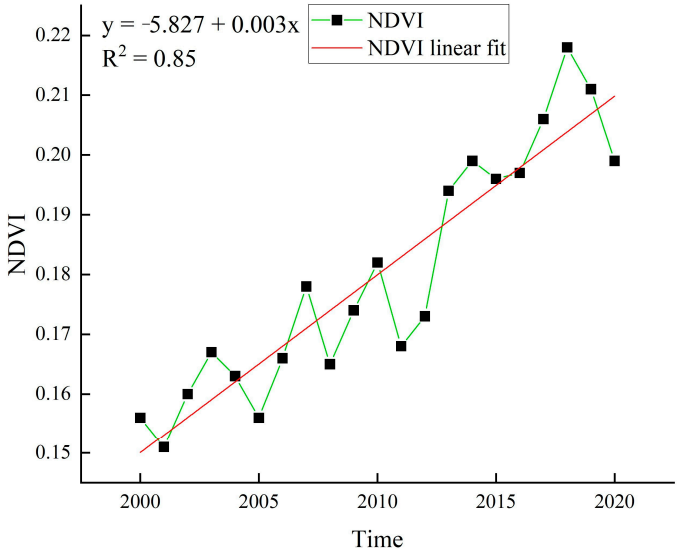

Figure 6. NDVI trend chart 2000–2019.

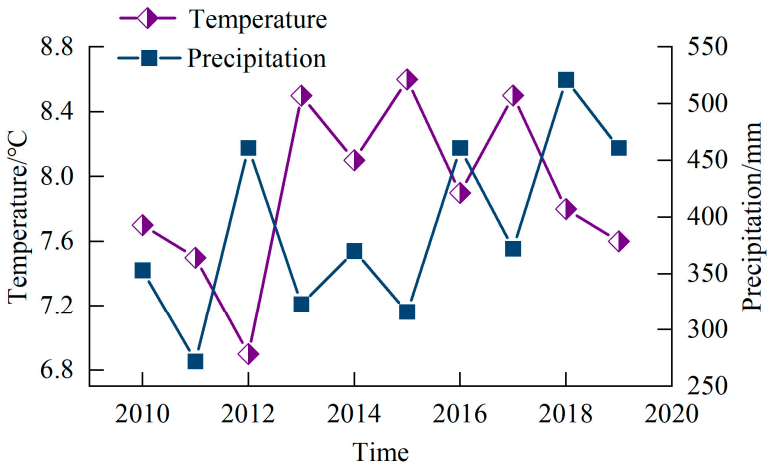

Figure 7. NDVI trend chart 2010–2019.

By using GEE for extracting the NDVI raster data, we observed a progressive decline in plant cover within the research area, namely, from the central region towards the northeast and southwest directions. Using a significance level of $\alpha = 0.05$, we categorized the change in vegetation cover into nine classes: highly significant increase, significant increase, marginally significant increase, non-significant increase, no change, non-significant decrease, marginally significant decrease, significant decrease, and highly significant decrease.

We used the Theil–Sen median trend value analysis in combination with the Mann–Kendall non-parametric test to accomplish this.

The observed trends in the study field exhibited substantial disparities in their upward and downward trajectories from 2000 to 2020. Merely a minuscule fraction of these areas saw a decrease in vegetation coverage, whereas a significant enhancement was seen in 99.28% of the sites. This pertains to the State's efforts in constructing and conserving the environment. The vegetation cover in the western region is experiencing a remarkable increase, indicating the clear effectiveness of the ecological protection project. Meanwhile, the vegetation cover in the eastern region is also growing significantly, primarily due to the time required for construction and ecological protection projects.

Upon comparing the NDVI trends for 2000 and 2020, we found no noticeable fluctuations in the growth rate of the plant cover over 20 years. Conversely, the vegetation cover exhibited uninterrupted growth over this period. Figure 8 depicts the geographical and temporal fluctuations of NDVI in the study region, indicating that the western section exhibits a dense population, larger cultivated land, and much more rapid vegetation development compared to the eastern section. These findings indicate that enhancing the vegetation is a significant outcome of the ecological restoration endeavor.

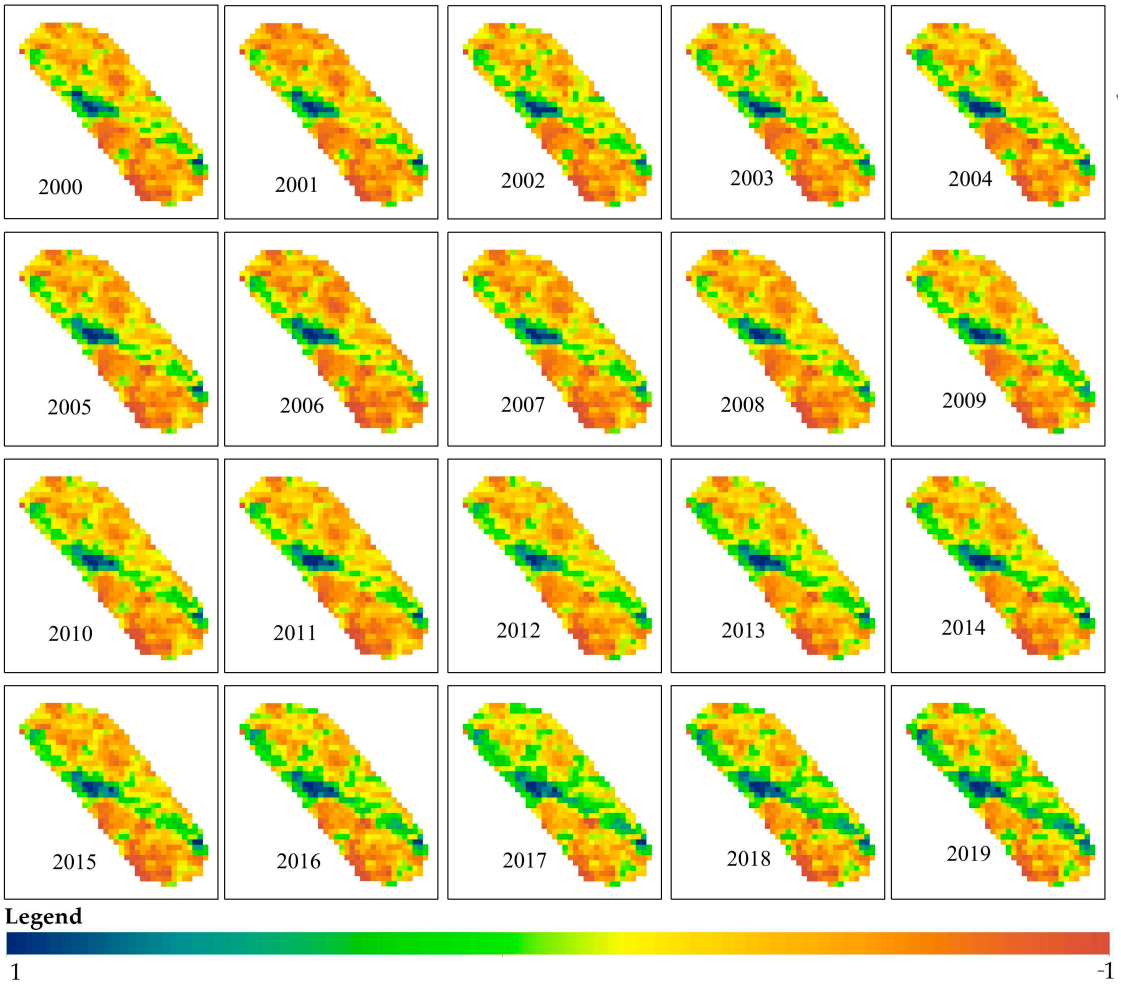

Figure 8. Distribution of NDVI time series in Ha Cai Tou water source area.

We gathered multispectral data in the research region between 12 March 2021 and 25 August 2023, yielding five indicators: Green Normalized Difference Vegetation Index (GNDVI), Leaf Chlorophyll Index (LCI), Normalized Difference Red Edge Index (NDRE), NDVI, and Optimized Soil Adjusted Vegetation Index (OSAVI). As seen in Figure 9, the

corresponding yearly mean values of these indicators were 0.23, 0.04, 0.03, 0.21, and 0.1. The findings indicated that there was not enough plant cover in the Ha Cai Tou Dang water source area. Low levels of vegetation biomass and health were indicated by low values of the vegetation cover coefficient and chlorophyll content coefficient. It was discovered that the plants were undernourished and in poor growing conditions. The research area's low biomass and unhealthy vegetation may be related to unfavorable ecological circumstances and arid summers in the sandy regions, which hurt the state of the plant. These results are critical to the preservation of ecological habitats in the Ha Cai Tou Dang water source area in the future.

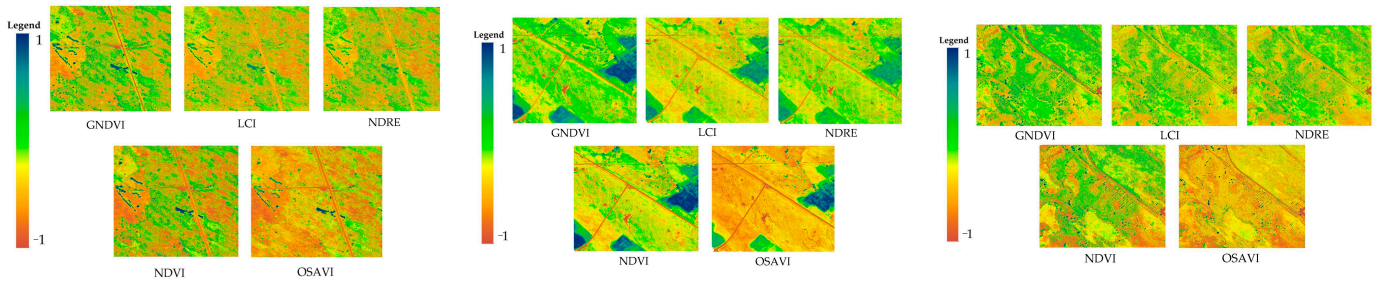

Figure 9. Extraction of GNDVI, LCI, NDRE, NDVI, and OSAVI aerial data in the study area.

3.3. Estimation of Vegetation Phenology Parameters and Analysis of the Influence of Ecological Factors

This work used NDVI data from the Global Inventory Mapping and Monitoring work (GIMMS) spanning from 2000 to 2020 to analyze the yearly changes in vegetation indices. The analysis employed a double Logistic function to explain the annual development of these indices. Furthermore, Figure 10 provides a comprehensive depiction of the procedure for determining the quantity of weather via the utilization of dual Logistic smoothing and computerized weather extraction methodologies. The Levenberg–Marquardt technique was used to optimize the fitting of the time series. The mean SOS and EOS of the growing season for the Ha Cai Tou Dang water source area were retrieved for the distribution locations. Furthermore, the Enhanced Vegetation Index (EVI) was computed to provide a more precise representation of the vegetation's growing conditions and overall health at each location. We conducted an estimation of the SOS and EOS for each site and then determined the length of the vegetation growth season. The research revealed that the SOS occurred on the 182nd day of the year at the six monitoring locations, while the EOS occurred on the 270th day. This indicates that, on average, the vegetation growth season lasted for 88 days. The highest EVI is normally seen in August. However, aerial images revealed that even though it was the height of the growing season, plant growth at this time was suboptimal. The groundwater level data collected in 2020 revealed an average depth to groundwater of 8.5 m, which is significantly above the maximum threshold of 7 m necessary for the establishment of plants. These findings suggest that the Ha Cai Tou Dang water source area location has a very brief vegetation growing season, and the soil and climatic conditions may not be conducive to plant development. The presence of EVI peaks does not indicate the most favorable vegetation growth, as it can be affected by various ecological or environmental factors, such as the depth of submerged groundwater. When water tables are deeply buried, vegetation may face limitations in accessing sufficient water and nutrients, leading to subpar growth.

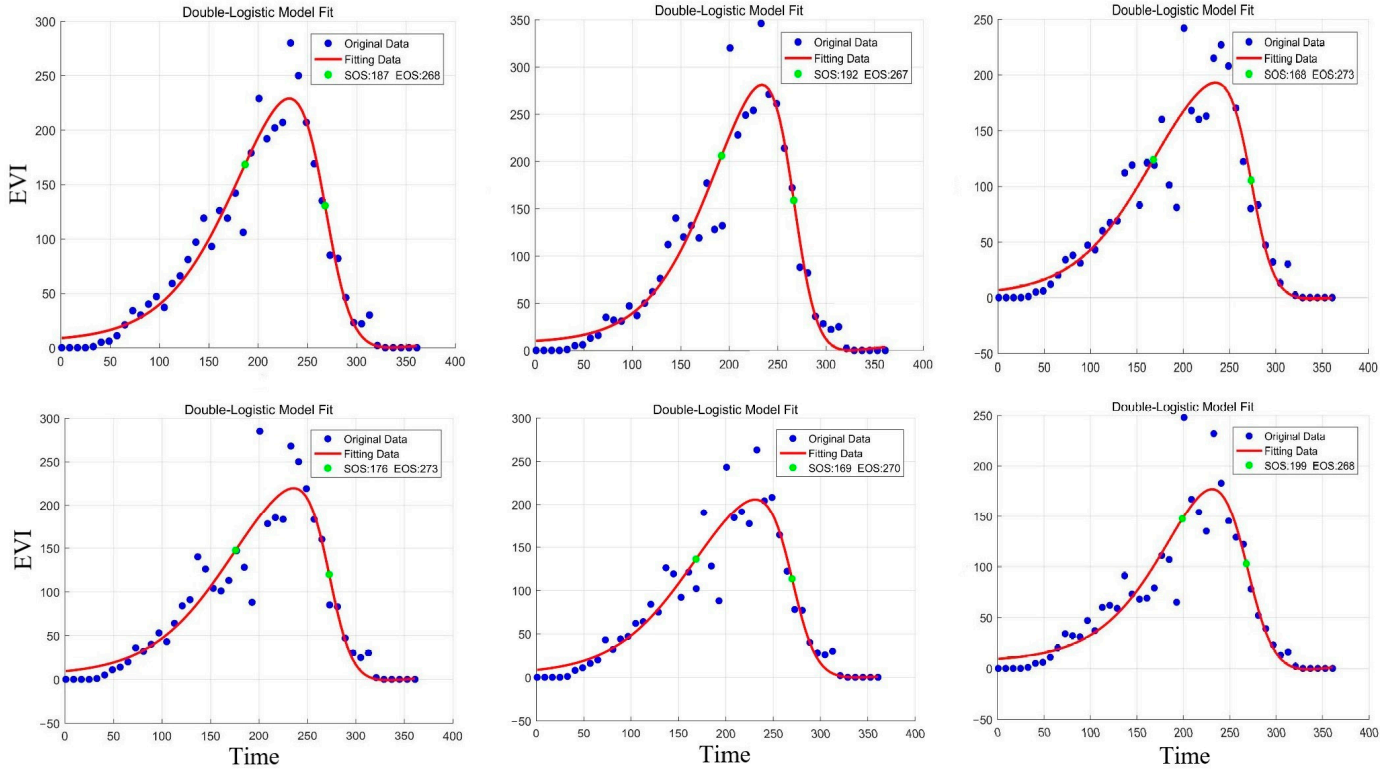

Figure 10. Annual evolution of surface phenological parameters with a double logistic function.

3.4. An In-Depth Analysis of the Relationship between Normalized Difference Vegetation Index (NDVI) and Land Surface Temperature (LST)

This study utilized GEE to conduct a comprehensive analysis of the NDVI in the study area from 2000 to 2020. We also obtained the corresponding maximum and minimum surface temperatures (LST) at a resolution of 500 m, as shown in Figure 10. By analyzing the yearly LST data from 2000 to 2019 and combining it with the NDVI, we were able to compute the TVDI for the research region from 2001 to 2020. This was achieved by using equations that accounted for both dry and wet conditions. Figure 11 illustrates the change in TVDI over 20 years. The investigation revealed a notable inverse association between the normalized NDVI and the highest surface temperature (Ts_{max}). This correlation was seen within the NDVI values ranging from 0.25 to 0.3. The data were further reinforced, indicating a notable inclination for the Ts_{max} values to diverge from the dry boundary, and the pace of decline increased in comparison to the preceding one. As the NDVI grew, the range between the highest and lowest temperatures diminished, resulting in the formation of a triangular feature space. Both the dry and wet margins exhibited negative slopes, suggesting a decline in surface temperature as the NDVI increased. Additionally, we saw a significant reduction in the temperature difference throughout the 20 years. This tendency suggests that the environment in the study region is progressively becoming more humid, which in turn will create more favorable circumstances for future plant development.

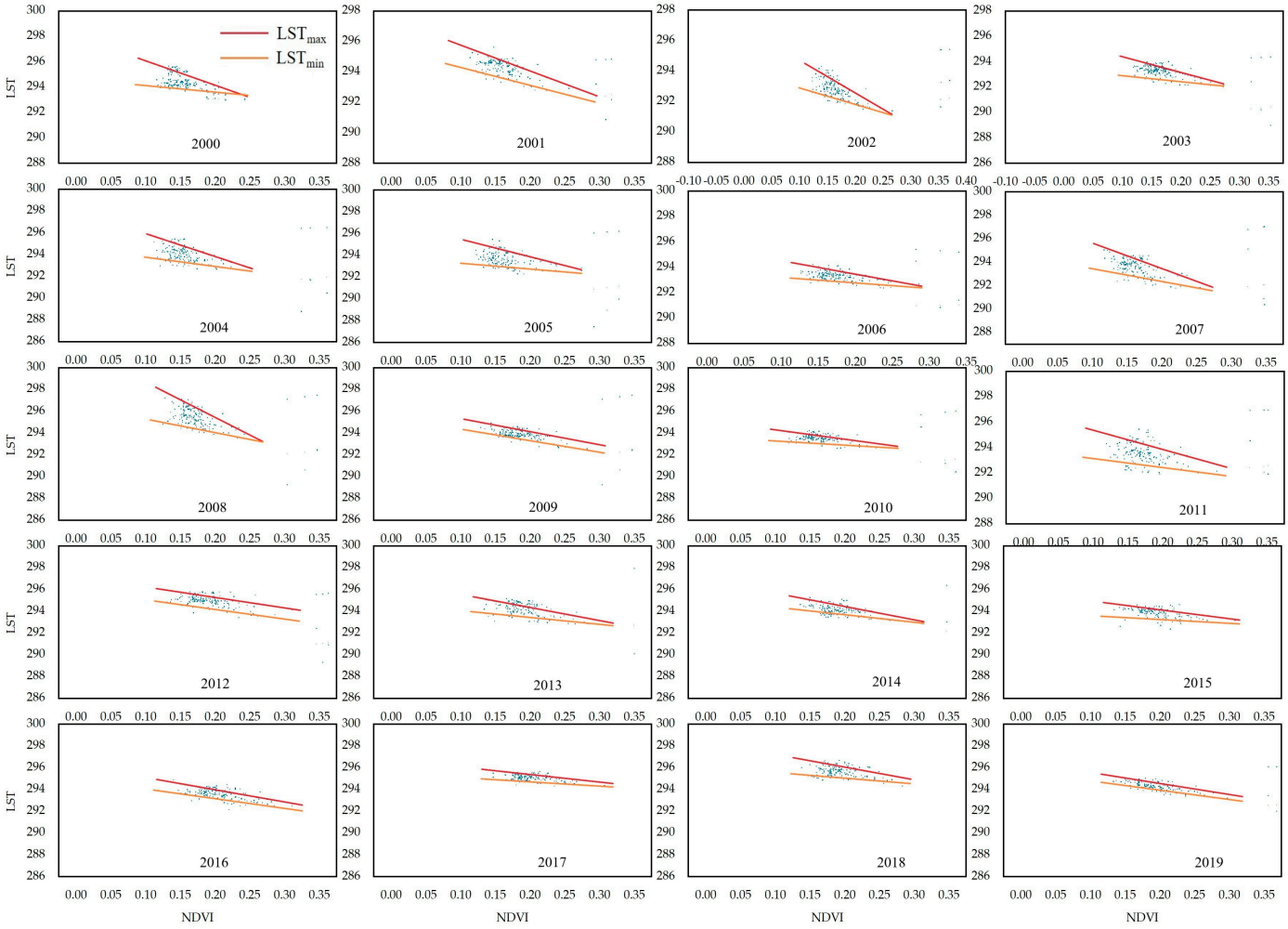

Figure 11. Spatial fit of NDVI-T_S features, 2000–2019.

3.5. Long-Term Monitoring and Analysis of Vegetation Dynamics and Its Drought Response

Significant ecological changes were seen via long-term monitoring of plant dynamics and responses to drought in the Ha Cai Tou Dang water source area throughout historical periods. The study involved calculating monthly mean values of various indices, including TVDI, NDVI, VSWI, VHI, TCI, and VCI, using remotely sensed data from 2000 to 2020. Figure 12 provides a comprehensive depiction of the quantitative analysis findings for VSWI, VHI, TCI, and VCI across the last two decades. The research revealed a notably increasing trend in the VSWI from January to February, followed by steady growth from March to December and a subsequent quick decline towards the end of the year. The observed variation pattern likely represents the vegetation's reaction to the restoration of moisture in spring and the prevailing climatic conditions in summer and autumn. It is important to mention that the average VSWI value remained below 0.12 throughout the year, highlighting the significant water shortage in the area. Both VHI and TCI exhibited progressive upward trends from January to August, followed by steady declines in the subsequent months, which aligns with typical seasonal growth trends. The VCI had a distinct non-linear pattern, unlike the other indices, which may be attributed to the combined effects of rainfall, temperature fluctuations, and changes in human land use.

Subsequent examination revealed the notable adverse effect of the year 1990, which saw the most intense drought stress, on the vegetative health of the Ha Cai Tou Dang water source area. This was evident in the very low values of NDVI, VSWI, VHI, and VCI, as well as unusually high values of TCI and TVDI. The vegetation was significantly impacted by the severe weather conditions seen during this time, resulting in long-term

repercussions. The region's agricultural development was significantly limited by climatic factors such as precipitation, temperature, and sun radiation. The limited amount of rainfall and cold temperatures throughout the spring hindered the development of vegetation. However, the rising VSWI trend demonstrated the plants' susceptibility to early spring moisture levels. Throughout the summer season, the rise in temperature and rainfall facilitated the proliferation of plant life, as seen by the elevation of VHI, VSWI, and VCI indices. Conversely, the decline in temperatures and precipitation throughout autumn signaled a premature conclusion to the vegetative cycle. Positive trends in NDVI over time indicate a rise in plant regeneration and improvement in ecosystem resilience. Furthermore, improvements in grazing management, such as the enforcement of grazing prohibitions and the adoption of rotational grazing systems, have effectively mitigated the negative impacts of overgrazing on soil and vegetation deterioration. The use of these eco-logical restoration strategies has led to the enhancement of vegetation indices such as VHI, VSWI, and VCI. The preservation of biodiversity and the evaluation of adaptive characteristics of plant types are crucial components of future study. Furthermore, conducting a thorough examination of the relationship between TCI and VHI will provide valuable insights for a more profound comprehension of the effects of climate change on vegetation health. An in-depth evaluation of these dynamic indicators will provide a more precise depiction of the vegetation's ecological condition in the Ha Cai Tou Dang water source region. This assessment will also establish a scientific foundation for environmental management and ecosystem rehabilitation efforts in the area.

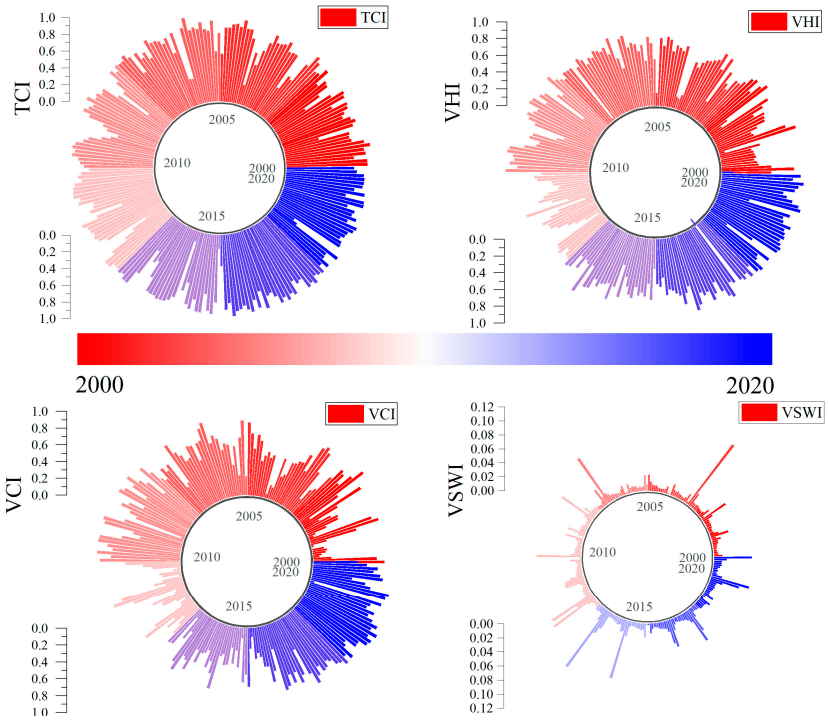

Figure 12. TCI, VHI, VCI, and VSWI, 2000–2020.

Figure 13 presents the Mantel test analysis of TVDI with NDVI, VSWI, TCI, VHI, VCI, precipitation, and temperature over a temporal scale. Our analysis revealed that the R-values of the Mantel tests conducted on the Ha Cai Tou Dang water source area were consistently below 0.2. This suggests a weak linear association between the variables under investigation, as seen in Figure 13. Nevertheless, there was a meaningful correlation between TVDI and TCI, suggesting that while their linear link is not strong, there could exist other sorts of interactions between them, such as non-linear or complex interaction relationships. A robust linear correlation was also seen between VSWI and both TCI and temperature. VSWI, or the Vegetation Water Supply Index, serves as a measure of the

current condition of vegetation water supply. On the other hand, TCI, or the Temperature Condition Index, serves as a measure of the current condition of the surface temperature. The strong linear association suggests a tight correlation between the water supply of vegetation and the surface temperature. This might be attributed to the significant impact of plant transpiration on the surface temperature. Furthermore, we discovered a robust correlation between VHI and both temperature and VCI. The VHI serves as a metric for assessing the overall health of vegetation, while the VCI is a metric specifically focused on evaluating plant cover. The robust linear correlation suggests a significant association between the health and coverage of vegetation and temperature, likely attributed to the substantial impact of temperature on the development and physiological functions of vegetation.

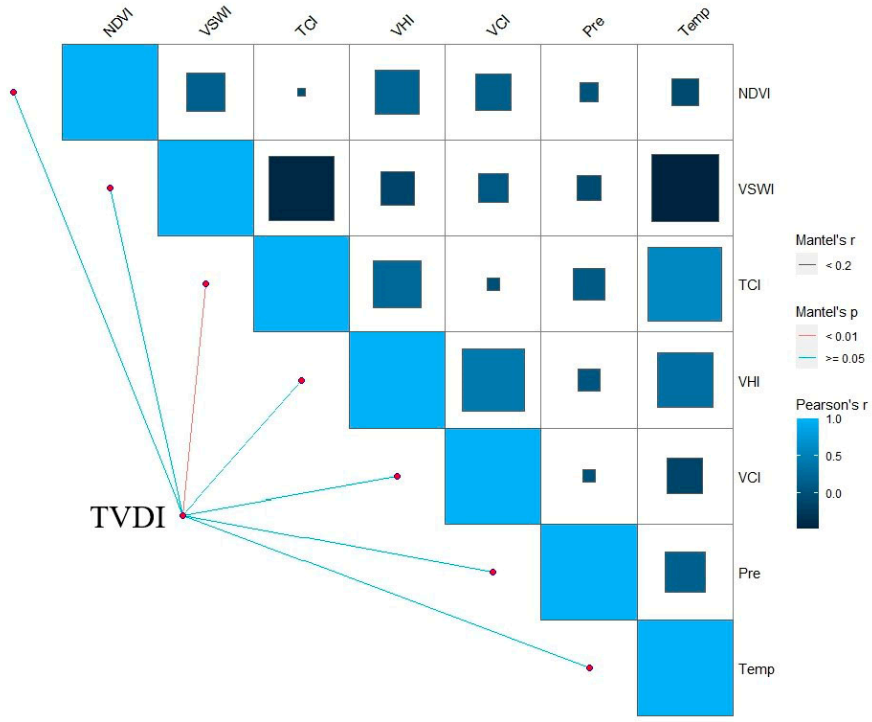

Figure 13. TVDI with NDVI, VSWI, TCI, VHI, VCI, precipitation, temperature temporal-scale Mantel test analysis.

3.6. Accurate Long Sequence Prediction Based on STL-EMD-Informer

This study focused on the Ha Cai Tou Dang water source area and analyzed 228 months (7305 days) of TCI data, from 1 January 2000 to 31 December 2019. The TVDI, which is primarily influenced by meteorological data, was examined. The meteorological data considered in this analysis included air temperature. It is important to take into account the meteorological factor conditions when predicting outcomes.

The experimental environment consisted of Python 3.8 and the PyCharm 3.8.1 framework, and the operating system environment was Windows 11 with 16GB of RAM.

Based on the meteorological and TCI data of the prediction model, this paper modified its hyperparameters for accurate predictions. The hyperparameters were adjusted based on the training results of the prediction model, and the final hyperparameters were set as follows: The learning rate was set at 0.0001, the number of iterations was 30, the batch size was 128, and the activation function used was GELU.

To validate the efficacy of the proposed prediction method, four widely utilized evaluation metrics were chosen to assess the model's prediction performance from various angles. These metrics included mean absolute error (MAE), mean square error (MSE), root

mean square error (RMSE), and MAPE. The prediction accuracy of the model increased as the evaluation indices decreased. The calculating method for these indices was as follows:

$$e_{MAE} = \frac{1}{n}\sum_{i=1}^{n}|y_i - \hat{y}_i| \tag{5}$$

$$e_{MSE} = \frac{1}{n}\sum_{i=1}^{n}|y_i - \hat{y}_i|^2 \tag{6}$$

$$e_{RMSE} = \sqrt{\frac{1}{n\sum_{i=1}^{n}(|y_i - \hat{y}_i|)^2}} \tag{7}$$

$$e_{MAPE} = \frac{1}{n}\sum_{i=1}^{n}|y_i - \hat{y}_i|/y_i \tag{8}$$

where: y_i is the true value of the original data. $\hat{y}_i$ is the predicted value of the original data. n is the test sample size. i is the test sample point sequence number.

Initially, we conducted an STL primary decomposition of the TVDI data, and the outcomes of the decomposition are shown in Figure 14. Figure 14 clearly illustrates that the decomposition yielded trend components that exhibited upward and downward trends for the original series. In contrast, the seasonal components had more consistent and periodic waveforms, while the residual components exhibited greater fluctuations without any discernible pattern.

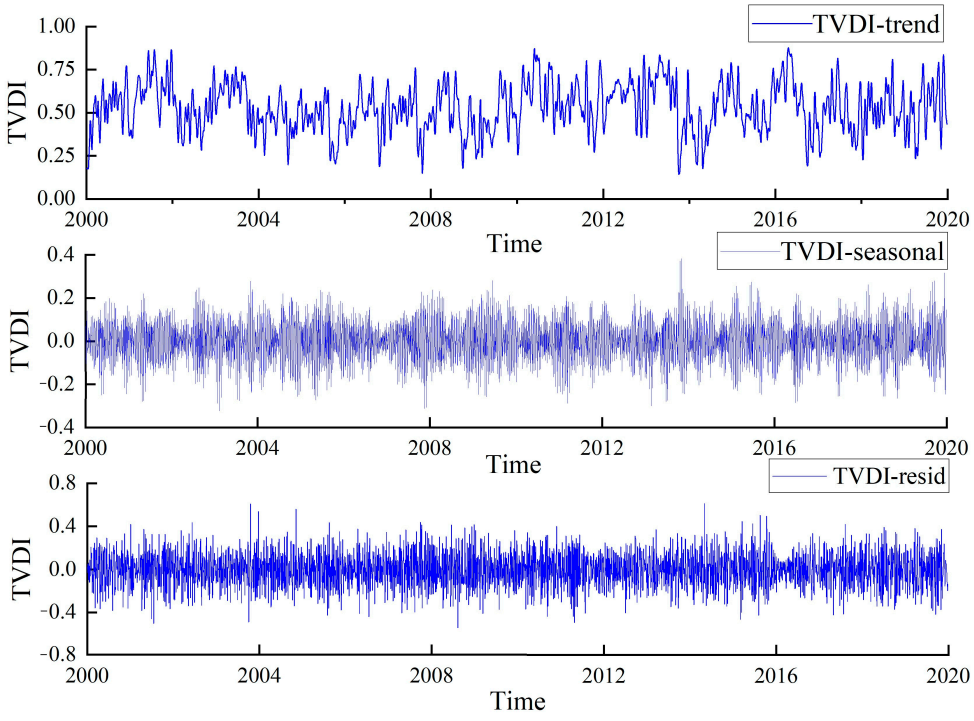

Figure 14. STL decomposition diagram.

Our analysis revealed that the residual component, albeit being more volatile, nevertheless has valuable information and unexplored patterns. To further investigate this, we subjected it to two rounds of EMD. The decomposition results are shown in Figure 15. The residual component of STL was divided into 10 intrinsic modal components. We included the prediction of the Informer model by reconstructing these components as prediction data. Finally, the prediction data were used to synthesize the TVDI.

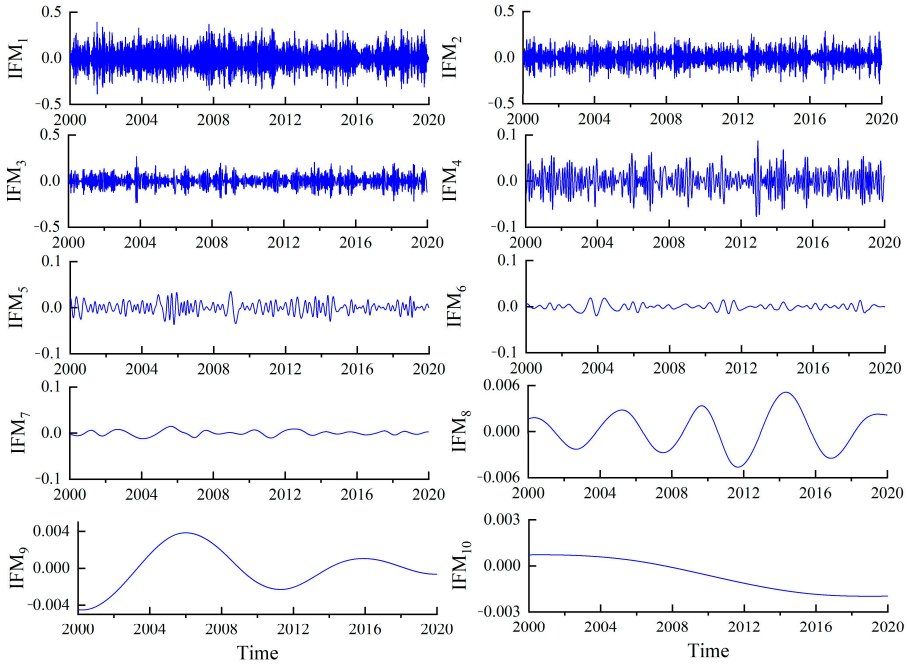

Figure 15. EMD decomposition diagram.

This work presents a prediction validation experiment where we used deep learning to test the accuracy of the prediction model. We used daily mean temperature, TCI, and TVDI data from 2000–2018. Figure 16 illustrates the prediction error plot for the STL-EMD-Informer model.

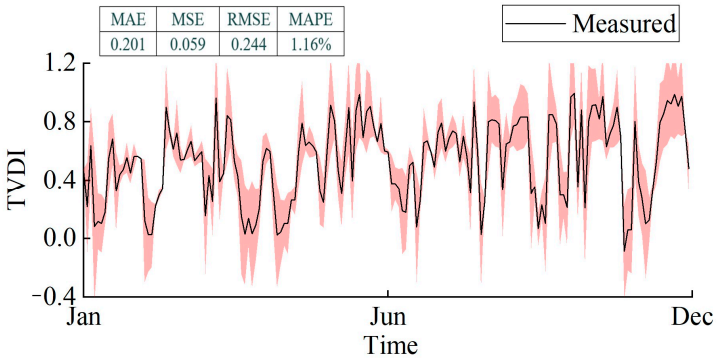

Figure 16. STL-EMD-Informer model error plot.

The prediction error values of MAE, MSE, RMSE, and MAPE for the results predicted by the STL-EMD-Informer model, as shown in Figure 16, were 0.201, 0.059, 0.224, and 1.16%, correspondingly, when compared to the true data. The mean absolute error was a mere 1.16%. Our enhanced Informer model, which utilized STL-EMD decomposition of the Transformer, provided compelling evidence of its accuracy in fitting the actual data curve. Our prediction model demonstrated superior performance to the old model, with reduced error and faster computing time, thereby confirming its viability. Hence, the model may be more effectively used to forecast the future trajectory of TVDI.

This work used the STL-EMD decomposition technique to integrate the Informer model and input the daily mean temperature, TVDI data, and NDVI data spanning from 2000 to 2020 for deep learning. The primary objective was to forecast the TVDI trend for the next decade. The maximum TVDI value for each year in the forecast results was around 0.7, similar to the maximum TVDI values seen in previous years in the input data. Figure 17 predicts the NDVI-TVDI for the whole year in an accurate manner, and the similarity with

previous TVDIs further validates the reliability of the model. According to the data in Figure 18, the forecast findings indicate that the TVDI trend will remain stable over the next decade, although the TVDI values will be consistently higher throughout the year. The linear fitting equations of TVDI exhibit smooth slopes, indicating that the anticipated changes over the next 10 years will be very small.

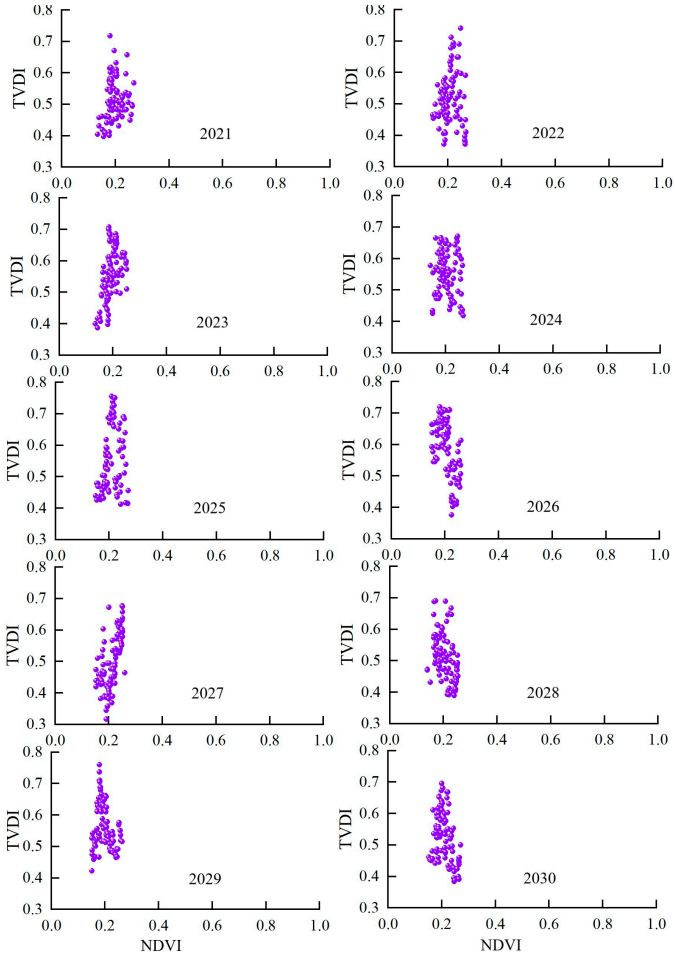

Figure 17. TVDI-NDVI feature space map.

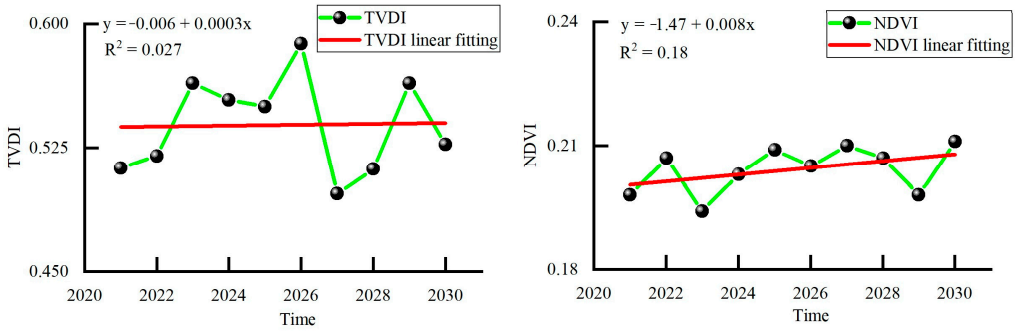

Figure 18. TVDI vs. NDVI trend forecast, 2021–2030.

4. Discussion

4.1. Characterization of Changes in Vegetation Trends

From 2000 to 2019, our analysis found little change in land use patterns in the region under investigation, marked by a tiny decline in grasslands and a steady rise in bare terrain. This phenomenon may be attributed to excessive grazing operations in the region,

leading to the degradation of pastureland [36]. The primary factors contributing to this phenomenon are likely the severe climate of the area, together with excessive grazing and unsustainable land reclamation for pasture purposes, among other factors [37]. However, the regional NDVI shows a consistent upward trend, notably in the western portion of the area, where a substantial enhancement in plant density is particularly prominent. The eastern part of the region also exhibits an inclination towards increased vegetation growth. This may be attributed to the favorable impact of the warmer and wetter climate pattern on vegetation growth in the northwestern part of the region. Additionally, it could be influenced by the higher proportion of arable land, the greater concentration of the population, and the allocation of resources.

Through the examination of multispectral remote sensing data, we have determined that the vegetation in the area has relatively low coverage, inadequate chlorophyll content, deficient plant nutrition, and concerning growth circumstances. The occurrence of this phenomenon may be attributed to the submergence of groundwater at a significant depth in the region, along with very high temperatures during the summer season. These factors together contribute to the degradation of the plant development conditions [38]. Cold and low temperatures may greatly hinder plant output, particularly by causing shorter plant growth cycles and higher apomixis [39].

The climatic characterization provides further evidence of the temporary nature of the vegetation growing season and the suboptimal values of the EVI, indicating that the total vegetation growth in the area is not optimal. The presence of water tables, shortages in soil nutrients, and restrictions in temperature at depths below the surface likely had a substantial effect on the availability of water and nutrients to plants, which in turn played a crucial role in the inadequate development of vegetation [40].

4.2. Vegetation Drought Characterization

An examination of the association between NDVI and Ts_{max} in the study region revealed a certain degree of negative connection between the two variables. The negative connection was especially notable within the NDVI range of 0.25 to 0.3. This indicates that when Ts_{max} rose, there was a deterioration in drought conditions in vegetation, accompanied by a considerable decline in NDVI values. This implies that, as temperatures rise, plant growth will be adversely impacted, resulting in higher rates of transpiration and excessive water loss. This effect was particularly pronounced when the Normalized Difference Vegetation Index (NDVI) fell within the sensitive range of 0.25 to 0.3, where vegetation demonstrates heightened sensitivity to temperature fluctuations [40]. Consequently, these changes in vegetation can indirectly influence surface temperatures through shading effects. Within this specific range of NDVI values, vegetation is likely in a crucial phase of development [41]. Even small fluctuations in temperature may have substantial effects on plant growth, particularly in dry regions, where elevated temperatures can lead to soil dehydration and therefore influence vegetation.

Furthermore, the notable pattern in the departure of maximum surface temperature (Ts_{max}) towards aridity suggests that higher temperatures expedite the evaporation of soil moisture, resulting in soil desiccation. This, in turn, hampers plant development and causes a decline in NDVI values. Nevertheless, the simultaneous negative slopes of the dry and wet margins suggest that the surface temperature decreased as the plant cover increased, hence promoting more favorable environmental conditions for future vegetation development [42].

The annual mean monthly value of the VSWI in the region was below 0.12, highlighting the area's limited availability of water resources. Meanwhile, the VHI and surface TCI displayed predictable patterns of change over the seasons. On the other hand, the VCI showed irregular variations, which could be attributed to the combined effects of factors such as rainfall, temperature fluctuations, and human-induced changes in land use. These findings suggest that colder winter temperatures lead to reduced vegetation growth, while hotter summer temperatures lead to higher rates of vegetation transpiration and increased

water stress. These effects are caused by a combination of factors, including precipitation, temperature variations, and human-induced changes in land use. In 1990, the abnormally low values of NDVI, VSWI, VHI, and VCI were accompanied by abnormally high values of TCI and TVDI. This suggests that the drought in that year had a substantial adverse effect on the vegetation health of the Ha Cai Tou Dang water source area. Furthermore, this severe climatic event had a lasting impact on the vegetation, as indicated by Sun et al. [43].

We have discovered strong associations between TVDI and TCI, as well as temperature. These findings indicate that drought and high-temperature circumstances have a substantial influence on the development and overall well-being of plants. Additionally, they may be used to identify water stress and provide guidance in managing drought situations [44]. Hence, the vegetation in the area must exhibit adaptability to temperature fluctuations by adjusting its physiological response to temperature variations to mitigate the effects of severe climatic conditions on vegetation and agriculture [45,46]. These results provide vital knowledge on how climatic conditions, such as rainfall, temperature, and sunlight, may significantly restrict crop development in the area. They also provide crucial information for agricultural production and management methods.

4.3. Accurate Long-Time Series STL-EMD-Informer Modeling

Precise forecasting of the TVDI is crucial for maintaining ecosystem health, reducing drought, and supporting sustainable development. Zhang et al. established the dependability of SVM in replicating the NDVI time series, but with an accuracy of only 86% throughout the validation period [27]. Zhuang et al. used CA–Markov modeling to forecast the net primary production (NPP) of vegetation. Their geographical simulation exhibited a kappa value of 0.8776, indicating that the model has a strong predictive capacity [29].

However, when compared to conventional machine learning techniques, deep learning has superior learning and fitting skills, particularly in its capacity to analyze and forecast extensive time series data. This study utilized the Informer model, which is a proficient LSTM architecture that integrates the STL-EMD quadratic decomposition and Transformer-based enhancements. The objective was to analyze deep meteorological factors such as temperature, TVDI, TCI, and NDVI data from 2000 to 2019. Additionally, a meticulous optimization of the hyperparameters was conducted. The model's probabilistic sparse self-attention mechanism efficiently addressed the non-stationarity and complexity of the original time-series data. Additionally, it extracted the inherent relevant information and rules, resulting in a substantial improvement in prediction accuracy.

The Informer model's exceptional performance lies in its ability to effectively learn and utilize the unpredictable patterns in meteorological factor data. Additionally, it retains crucial information from the original data and reduces data volatility by implementing a probabilistic sparse self-attention mechanism. Consequently, this model significantly enhanced the accuracy of TVDI prediction. The Informer model, when used for TVDI prediction, achieved a significant reduction in the MAPE value to 1.16%, indicating exceptional prediction ability. This study offers a highly effective scientific approach for predicting TVDI in China and globally, with significant theoretical and practical implications.

5. Conclusions

The land use composition of the Ha Cai Tou Dang water source area is mostly composed of grassland, with bare ground, shrubland, farmland, and woodland being secondary land use categories. Over the last several years, there have been mild alterations in the land cover of the region, characterized by a small decline in grassland and a corresponding rise in bare land. Through the analysis of the NDVI, we noted a gradual decline in NDVI values from the central region toward the northeast and southwest. However, the overall trend showed increased vegetation cover, with a fluctuation range of $0.003a^{-1}$. This indicates a general improvement in vegetation cover during the monitoring period, with a significant increase observed in approximately 99.28% of the area. By analyzing the physical characteristics, we determined that the start of the growing season (SOS) occurred, on

average, on the 182nd day of the year. In contrast, the EOS occurred on the 270th day of the year at the six monitoring sites. This indicates that the vegetation's growing season lasted, on average, for 88 days. The vegetation's development may be constrained by the greater distance to the groundwater, which restricts its availability to water and nutrients. Through an examination of the TVDI spanning from 2000 to 2020, we determined that the environment in the research region has become progressively more humid each year, while the temperature disparity has consistently diminished. Furthermore, this is reinforced by the robust correlation between TVDI and both the surface TCI and temperature.

The study utilizes the STL-EMD-Informer model to address various drawbacks associated with conventional Transformer models in long-series time prediction. These drawbacks include the ineffective handling of long and LSTF, excessive memory usage, limitations of the codec architecture, and reduced speed in predicting long time series. The model demonstrates exceptional aptitude in handling unpredictable meteorological data, and its probabilistic sparse self-attention mechanism effectively retains crucial information from the original data while mitigating data volatility, resulting in precise forecasting of long time series (MAPE = 1.16%).

This work successfully integrates the examination of past data with the forecasting of future patterns, offering fresh insights and methodologies for predicting crop output, NDVI, and TVDI. This innovative approach to agricultural production and management has the potential to enhance efficiency and sustainability in agriculture. This discovery not only has immense significance in the realm of scientific investigation, but also carries crucial ramifications for practical implementations.

Author Contributions: The contributions of H.Z., H.H. and C.T. were involved in designing the manuscript; R.L. carried out this experiment; H.Z. and R.L. analyzed the data and wrote the manuscript. All authors have read and agreed to the published version of the manuscript.

Funding: Ordos Water Conservancy Science and Technology Project "Research on the Development of Monitoring and Early Warning System for Groundwater Exploitation and Utilization and Ecological Environment in Maowusu Sandland (Research on Monitoring and Early Warning of Water Supply Sources in Ordos Central City)" (MK20210222); Key Special Project of the "Science and Technology for the Development of Mongolia" Initiative—Technology and Demonstration of Intensive and Efficient Utilization of Water Resources in the Maowusu Sandland Based on Ecological Security (2021EEDSCXSFQZD010).

Data Availability Statement: The data presented in this study are available on request from the corresponding author. The data are not publicly available due to privacy.

Conflicts of Interest: The authors declare no conflicts of interest.

References

1. Kalisa, W.; Zhang, J.; Igbawua, T.; Ujoh, F.; Ebohon, O.J.; Namugize, J.N.; Yao, F. Spatio-temporal analysis of drought and return periods over the East African region using Standardized Precipitation Index from 1920 to 2016. *Agric. Water Manag.* **2020**, *237*, 106195. [CrossRef]
2. Bayarjargal, Y.; Karnieli, A.; Bayasgalan, M.; Khudulmur, S.; Gandush, C.; Tucker, C.J. A comparative study of NOAA–AVHRR derived drought indices using change vector analysis. *Remote Sens. Environ.* **2006**, *105*, 9–22. [CrossRef]
3. Guo, Y.; Han, L.; Zhang, D.; Sun, G.; Fan, J.; Ren, X. The Factors Affecting the Quality of the Temperature Vegetation Dryness Index (TVDI) and the Spatial–Temporal Variations in Drought from 2011 to 2020 in Regions Affected by Climate Change. *Sustainability* **2023**, *15*, 11350. [CrossRef]
4. Wang, X.; Li, Y.; Wang, X.; Li, Y.; Lian, J.; Gong, X. Temporal and Spatial Variations in NDVI and Analysis of the Driving Factors in the Desertified Areas of Northern China from 1998 to 2015. *Front. Environ. Sci.* **2021**, *9*, 633020. [CrossRef]
5. Huang, S.; Tang, L.; Hupy, J.P.; Wang, Y.; Shao, G. A commentary review on the use of normalized difference vegetation index (NDVI) in the era of popular remote sensing. *For. Res.* **2021**, *32*, 1–6.
6. Li, W.; Ni, L.; Li, Z.L.; Duan, S.B.; Wu, H. Evaluation of machine learning algorithms in spatial downscaling of MODIS land surface temperature. *IEEE J. Sel. Top. Appl. Earth Obs. Remote Sens.* **2019**, *12*, 2299–2307. [CrossRef]
7. Gao, Z.; Gao, W.; Chang, N.B. Integrating temperature vegetation dryness index (TVDI) and regional water stress index (RWSI) for drought assessment with the aid of LANDSAT TM/ETM+ images. *Int. J. Appl. Earth Obs. Geoinf.* **2011**, *13*, 495–503. [CrossRef]

8. Bento, V.A.; Gouveia, C.M.; DaCamara, C.C.; Libonati, R.; Trigo, I.F. The roles of NDVI and Land Surface Temperature when using the Vegetation Health Index over dry regions. *Glob. Planet. Change* **2020**, *190*, 103198. [CrossRef]
9. Fu, B.; Burgher, I. Riparian vegetation NDVI dynamics and its relationship with climate, surface water, and groundwater. *J. Arid. Environ.* **2015**, *113*, 59–68. [CrossRef]
10. Lin, M.; Hou, L.; Qi, Z.; Wan, L. Impacts of climate change and human activities on vegetation NDVI in China's Mu Us Sandy Land during 2000–2019. *Ecol. Indic.* **2022**, *142*, 109164. [CrossRef]
11. Oliveira, N.M.D.; Silva, R.M.D.; Brasil Neto, R.M.; Santos, C.A.G.; Vianna, P.C.G. Spatiotemporal patterns of agricultural and meteorological droughts using SPI and MODIS-based estimates over a Brazilian semiarid region: Study case of Upper Paraíba River basin. *Geocarto J. Int.* **2022**, *37*, 11590–11613. [CrossRef]
12. Sohail, M.T.; Manzoor, Z.; Ehsan, M.; Al-Ansari, N.; Khan, M.B.; Shafi, A.; Ullah, J.; Hussain, S.; Raza, D.; Usman, U.; et al. Impacts of urbanization, LULC, LST, and NDVI changes on the static water table with possible solutions and water policy discussions: A case from Islamabad, Pakistan. *Front. Environ. Sci.* **2023**, *11*, 1018500. [CrossRef]
13. Zheng, B.; Myint, S.W.; Thenkabail, P.S.; Aggarwal, R.M. A support vector machine to identify irrigated crop types using time-series Landsat NDVI data. *Int. J. Appl. Earth Obs. Geoinf.* **2015**, *34*, 103–112. [CrossRef]
14. Ye, W.A.N.G.; Haijing, S.H.I.; Yanmin, J.I.A.N.G.; Youfu, W.U.; Yuan, G.A.O.; Chengqin, D.I.N.G. Spatio-temporal Variation of Drought Characteristics and Its Influencing Factors in Loess Plateau Based on TVDI. *Nongye Jixie Xuebao/Trans. Chin. Soc. Agric. Mach.* **2023**, *54*, 184–195.
15. Lin, X.C.; Chen, J.J.; Lou, P.Q. Temporal and spatial changes of drought in beijing-tianjin-hebei region based on remote sensing technology. *Int. Arch. Photogramm. Remote Sens. Spat. Inf. Sci.* **2020**, *42*, 747–753. [CrossRef]
16. Gidey, E.; Dikinya, O.; Sebego, R.; Segosebe, E.; Zenebe, A. Analysis of the long-term agricultural drought onset, cessation, duration, frequency, severity, and spatial extent using Vegetation Health Index (VHI) in Raya and its environs, Northern Ethiopia. *Environ. Syst. Res.* **2018**, *7*, 13. [CrossRef]
17. Chen, S.; Zhang, L.; Tang, R.; Yang, K.; Huang, Y. Analysis on temporal and spatial variation of drought in Henan Province based on SPEI and TVDI. *Trans. Chin. Soc. Agric. Eng.* **2017**, *33*, 126–132.
18. Chen, D.; Lu, R.; Liu, X.; Ding, Z. Holocene Vegetation and climate reconstructions from pollen records in the mu us sandy land, China. *Catena* **2023**, *220*, 106698. [CrossRef]
19. Gao, P.; Du, W.; Lei, Q.; Li, J.; Zhang, S.; Li, N. NDVI Forecasting Model Based on the Combination of Time Series Decomposition and CNN–LSTM. *Water Resour. Manag.* **2023**, *37*, 1481–1497. [CrossRef]
20. Kattenborn, T.; Leitloff, J.; Schiefer, F.; Hinz, S. Review on Convolutional Neural Networks (CNN) in vegetation remote sensing. *ISPRS J. Photogramm. Remote Sens.* **2021**, *173*, 24–49. [CrossRef]
21. Li, X.; Yuan, W.; Dong, W. A machine learning method for predicting vegetation indices in China. *Remote Sens.* **2021**, *13*, 1147. [CrossRef]
22. Yu, W.; Li, J.; Liu, Q.; Zhao, J.; Dong, Y.; Wang, C.; Lin, S.; Zhu, X.; Zhang, H. Spatial–temporal prediction of vegetation index with deep recurrent neural networks. *IEEE Geosci. Remote Sens. Lett.* **2021**, *19*, 2501105. [CrossRef]
23. Navnath, N.N.; Chandrasekaran, K.; Stateczny, A.; Sundaram, V.M.; Panneer, P. Spatiotemporal Assessment of Satellite Image Time Series for Land Cover Classification Using Deep Learning Techniques: A Case Study of Reunion Island, France. *Remote Sens.* **2022**, *14*, 5232. [CrossRef]
24. Xiong, C.; Ma, H.; Liang, S.; He, T.; Zhang, Y.; Zhang, G.; Xu, J. Improved global 250 m 8-day NDVI and EVI products from 2000–2021 using the LSTM model. *Sci. Data* **2023**, *10*, 800. [CrossRef] [PubMed]
25. Liu, H.; Tang, Y.; Pu, Y.; Mei, F.; Sidorov, D. Short-term load forecasting of multi-energy in an integrated energy system based on multivariate phase space reconstruction and support vector regression mode. *Electr. Power Syst. Res.* **2022**, *210*, 108066. [CrossRef]
26. Wu, T.; Fu, H.; Feng, F.; Bai, H. A new approach to predict normalized difference vegetation index using time-delay neural network in the arid and semi-arid grassland. *Int. J. Remote Sens.* **2019**, *40*, 9050–9063. [CrossRef]
27. Zhang, Y.; Guo, L.; Chen, Y.; Shi, T.; Luo, M.; Ju, Q.; Wang, S. Prediction of soil organic carbon based on Landsat 8 monthly NDVI data for the Jianghan Plain in Hubei Province, China. *Remote Sens.* **2019**, *11*, 1683. [CrossRef]
28. Zhou, H.; Zhang, S.; Peng, J.; Zhang, S.; Li, J.; Xiong, H.; Zhang, W. Informer: Beyond efficient transformer for long sequence time-series forecasting. *Proc. AAAI Conf. Artif. Intell.* **2021**, *35*, 11106–11115. [CrossRef]
29. Zhuang, Z.; Zheng, X.; Chen, Z.; Jin, T. A reliable short-term power load forecasting method based on VMD-IWOA-LSTM algorithm. *IEEJ Trans. Electr. Electron. Eng.* **2022**, *17*, 1121–1132. [CrossRef]
30. Liang, P.; Yang, X. Landscape spatial patterns in the Maowusu (Mu Us) Sandy Land, northern China and their impact factors. *Catena* **2016**, *145*, 321–333. [CrossRef]
31. Khare, S.; Ghosh, S.K.; Latifi, H.; Vijay, S.; Dahms, T. Seasonal-based analysis of vegetation response to environmental variables in the mountainous forests of Western Himalaya using Landsat 8 data. *Int. J. Remote Sens.* **2017**, *38*, 4418–4442. [CrossRef]
32. Zhong, X.; Li, J.; Wang, J.; Zhang, J.; Liu, L.; Ma, J. Linear and Nonlinear Characteristics of Long-Term NDVI Using Trend Analysis: A Case Study of Lancang-Mekong River Basin. *Remote Sens.* **2022**, *14*, 6271. [CrossRef]
33. Yang, Y.; Wang, S.; Bai, X.; Tan, Q.; Li, Q.; Wu, L.; Tian, S.; Hu, Z.; Li, C.; Deng, Y. Factors affecting long-term trends in global NDVI. *Forests* **2019**, *10*, 372. [CrossRef]
34. Nietupski, T.C.; Kennedy, R.E.; Temesgen, H.; Kerns, B.K. Spatiotemporal image fusion in Google Earth Engine for annual estimates of land surface phenology in a heterogenous landscape. *Int. J. Appl. Earth Obs. Geoinf.* **2021**, *99*, 102323. [CrossRef]

35. Ye, Z.X.; Cheng, W.M.; Zhao, Z.Q.; Guo, J.Y.; Yang, Z.X.; Wang, R.B.; Wang, N. Spatio-Temporal characteristics of drought events and their effects on vegetation: A case study in southern Tibet, China. *Remote Sens.* **2020**, *12*, 4174. [CrossRef]
36. Liu, C.; Liu, J.; Zhang, Q.; Ci, H.; Gu, X.; Gulakhmadov, A. Attribution of NDVI Dynamics over the Globe from 1982 to 2015. *Remote Sens.* **2022**, *14*, 2706. [CrossRef]
37. Shammi, S.A.; Meng, Q. Modeling crop yield using NDVI-derived VGM metrics across different climatic regions in the USA. *Int. J. Biometeorol.* **2023**, *67*, 1051–1062. [CrossRef] [PubMed]
38. Hao, F.; Zhang, X.; Ouyang, W.; Skidmore, A.K.; Toxopeus, A.G. Vegetation NDVI is linked to temperature and precipitation in the upper catchments of the Yellow River. *Environ. Model. Assess.* **2018**, *17*, 389–398. [CrossRef]
39. Li, S.; Li, X.; Gong, J.; Dang, D.; Dou, H.; Lyu, X. Quantitative analysis of natural and anthropogenic factors influencing vegetation NDVI changes in temperate drylands from a spatial stratified heterogeneity perspective: A case study of Inner Mongolia Grasslands, China. *Remote Sens.* **2022**, *14*, 3320. [CrossRef]
40. Elsheery, N.I.; Sunoj, V.S.J.; Wen, Y.; Zhu, J.J.; Muralidharan, G.; Cao, K.F. Foliar application of nanoparticles mitigates the chilling effect on photosynthesis and photoprotection in sugarcane. *Plant Physiol. Biochem.* **2020**, *149*, 50–60. [CrossRef]
41. He, P.; Xu, L.; Liu, Z.; Jing, Y.; Zhu, W. Dynamics of NDVI and its influencing factors in the Chinese Loess Plateau during 2002–2018. *Reg. Sustain.* **2021**, *2*, 36–46. [CrossRef]
42. Mallick, J.; AlMesfer, M.K.; Singh, V.P.; Falqi, I.I.; Singh, C.K.; Alsubih, M.; Kahla, N.B. We are evaluating the NDVI–rainfall relationship in the Bisha watershed, Saudi Arabia using a non-stationary modeling technique. *Atmosphere* **2021**, *12*, 593. [CrossRef]
43. Sun, Z.; Mao, Z.; Yang, L.; Liu, Z.; Han, J.; Wanag, H.; He, W. Impacts of climate change and afforestation on vegetation dynamic in the Mu Us Desert, China. *Ecol. J. Indic.* **2021**, *129*, 108020. [CrossRef]
44. Wang, T.; Yang, M.; Yan, S.; Geng, G.; Li, Q.; Wang, F. Temporal and Spatial Vegetation Index Variability and Response to Temperature and Precipitation in the Qinghai-Tibet Plateau Using GIMMS NDVI. *Pol. J. Environ. Stud.* **2020**, *29*, 4385–4395. [CrossRef]
45. Meng, X.; Gao, X.; Li, S.; Lei, J. Spatial and temporal characteristics of vegetation NDVI changes and the driving forces in Mongolia during 1982–2015. *Remote Sens.* **2020**, *12*, 603. [CrossRef]
46. Pei, F.; Zhou, Y.; Xia, Y. Application of normalized difference vegetation index (NDVI) for the detection of extreme precipitation change. *Forests* **2021**, *12*, 594. [CrossRef]